The Astrophysical Journal Letters, 811:L3 (6pp), 2015 September 20 doi:10.1088/2041-8205/811/1/L3

SXDF-ALMA 1.5 arcmin^2 DEEP SURVEY: A COMPACT DUSTY STAR-FORMING GALAXY AT $z = 2.5$

Ken-ichi Tadaki[1], Kotaro Kohno[2,3], Tadayuki Kodama[4,5], Soh Ikarashi[6], Itziar Aretxaga[7], Stefano Berta[1], Karina I. Caputi[6], James S. Dunlop[8], Bunyo Hatsukade[4], Masao Hayashi[4], David H. Hughes[7], Rob Ivison[8,9], Takuma Izumi[2], Yusei Koyama[4], Dieter Lutz[1], Ryu Makiya[2], Yuichi Matsuda[4,5], Kouichiro Nakanishi[4,5,10], Wiphu Rujopakarn[11,12], Yoichi Tamura[2], Hideki Umehata[2,9], Wei-Hao Wang[13,14], Grant W. Wilson[15], Stijn Wuyts[1], Yuki Yamaguchi[2], and Min S. Yun[15]

[1] Max-Planck-Institut für extraterrestrische Physik (MPE), Giessenbachstrasse, D-85748 Garching, Germany; tadaki@mpe.mpg.de
[2] Institute of Astronomy, The University of Tokyo, 2-21-1 Osawa, Mitaka, Tokyo 181-0015, Japan
[3] Research Center for the Early Universe, The University of Tokyo, 7-3-1 Hongo, Bunkyo, Tokyo 113-0033, Japan
[4] National Astronomical Observatory of Japan, 2-21-1 Osawa, Mitaka, Tokyo 181-8588, Japan
[5] Department of Astronomical Science, SOKENDAI (The Graduate University for Advanced Studies), Mitaka, Tokyo 181-8588, Japan
[6] Kapteyn Astronomical Institute, University of Groningen, P.O. Box 800, 9700AV Groningen, The Netherlands
[7] Instituto Nacional de Astrofísica, Óptica y Electrónica (INAOE), Luis Enrique Erro 1, Sta. Ma. Tonantzintla, Puebla, Mexico
[8] Institute for Astronomy, University of Edinburgh, Royal Observatory, Blackford Hill, Edinburgh EH9 3HJ, UK
[9] European Southern Observatory, Karl-Schwarzschild-Strasse 2, Garching bei Munchen, Germany
[10] Joint ALMA Observatory, Alonso de Córdova 3107, Vitacura 763-0355, Santiago, Chile
[11] Department of Physics, Faculty of Science, Chulalongkorn University, 254 Phayathai Road, Pathumwan, Bangkok 10330, Thailand
[12] Kavli Institute for the Physics and Mathematics of the Universe (WPI), Todai Institute for Advanced Study, University of Tokyo, 5-1-5 Kashiwanoha, Kashiwa 277-8583, Japan
[13] Institute of Astronomy and Astrophysics, Academia Sinica, Taipei, Taiwan
[14] Canada–France–Hawaii Telescope, Waimea, HI, USA
[15] Department of astronomy, University of Massachusetts, Amherst, MA 01003, USA
Received 2015 June 1; accepted 2015 August 24; published 2015 September 11

ABSTRACT

We present the first results from the SXDF-Atacama Large Millimeter/submillimeter Array (ALMA) 1.5 arcmin^2 deep survey at 1.1 mm using ALMA. The map reaches a 1σ depth of 55 μJy/beam and covers 12 Hα-selected star-forming galaxies (SFGs) at $z = 2.19$ or $z = 2.53$. We have detected continuum emission from three of our Hα-selected sample, including one compact SFG with high stellar surface density, NB2315-07. They are all red in the rest-frame optical and have stellar masses of $\log(M_*/M_\odot) > 10.9$, whereas the other blue, main-sequence galaxies with $\log(M_*/M_\odot) = 10.0$–10.8 are exceedingly faint, $<290\,\mu$Jy (2σ upper limit). We also find the 1.1 mm brightest galaxy, NB2315-02, to be associated with a compact ($R_e = 0.7 \pm 0.1$ kpc), dusty star-forming component. Given a high gas fraction (44^{+20}_{-8}% or 37^{+25}_{-3}%) and high star formation rate surface density (126^{+27}_{-30} $M_\odot$ yr^{-1} kpc^{-2}), the concentrated starburst can build up within less than 50^{+12}_{-11} Myr a stellar surface density matching that of massive compact galaxies at $z \sim 2$, provided at least 19 ± 3% of the total gas is converted into stars in the galaxy center. On the other hand, NB2315-07, which already has such a high stellar surface density core, shows a gas fraction (23^{+8}_{-8}%) and is located in the lower envelope of the star formation main sequence. This compact, less SFG is likely to be in an intermediate phase between compact, dusty star-forming and quiescent galaxies.

Key words: galaxies: evolution – galaxies: high-redshift – galaxies: ISM

1. INTRODUCTION

One of the fundamental questions in galaxy formation is when and how massive galaxies are formed at high redshift. Massive quiescent galaxies (QGs) already existed at $z \geqslant 2$ when the cosmic star formation activity peaked (e.g., Kriek et al. 2009). They are extremely compact with an effective radius of only $R_e \sim 1$ kpc in the rest-frame optical, which is a factor of 4–5 smaller than the size of local QGs at similar stellar masses (e.g., Trujillo et al. 2007; van Dokkum et al. 2008; Newman et al. 2012). This discovery has challenged galaxy evolution theories and raised the major question of how the compact QGs subsequently grow in size. It has become widely accepted that the observed size evolution is due to a combination of two evolutionary channels: *slow* and *fast* modes. In the slow mode, new, larger quenched galaxies continuously add to the quiescent population at $0 < z < 2$ (e.g., Williams et al. 2010; Belli et al. 2015). In the fast mode, compact star-forming galaxies (SFGs) are quenched to become compact QGs at $z \sim 2$ and subsequently puff up through repeated dry minor mergers (e.g., Naab et al. 2009; van Dokkum et al. 2010). While the size growth of QGs has been partially understood, the formation mechanisms of compact stellar components, in the fast mode, remain poorly done.

Theoretical studies predict that a 1 kpc scale core can be produced by dissipative processes such as gas-rich major mergers or disk instability-driven inflow within galaxies (Wuyts et al. 2010; Bournaud et al. 2011; Dekel & Burkert 2014; Wellons et al. 2015). Such violent processes should happen on a short timescale so that external gas accretion does not re-grow galaxy disks. While typical massive SFGs have a large disk with $R_e \sim 4$ kpc at $z \sim 2$ (e.g., van der Wel et al. 2014), recent high-resolution Atacama Large Millimeter/submillimeter Array (ALMA) imaging reveals that submillimeter bright galaxies (SMGs) have a dusty star-forming core whose size is four times smaller than their stellar component (Simpson et al. 2015; see also Ikarashi et al. 2014). Moreover, massive compact SFGs have been discovered at $z \sim 2$ (e.g., Wuyts et al. 2011b; Barro et al. 2013; Tadaki et al. 2014) and their high stellar surface densities suggest that they can directly evolve into compact QGs without structural

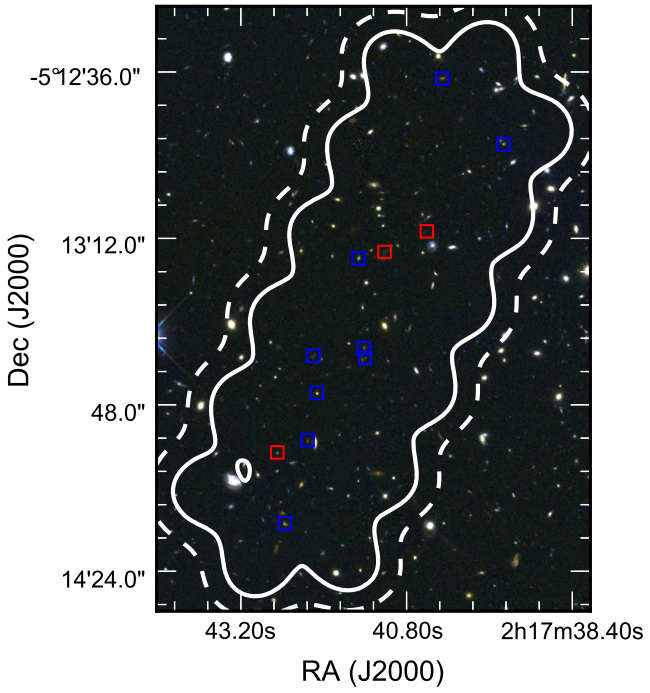

Figure 1. Twelve Hα-selected SFGs in the SXDF-ALMA 1.5 arcmin^2 deep field. Red and blue squares indicate 1.1 mm sources and non-detections, respectively. A white solid and white dashed line show the areas where the primary beam correction is below 20% and 50%, respectively.

transformation, simply by quenching star formation. The number density evolution of compact SFGs supports the production of the observed number densities of compact QGs over the same epoch with a quenching timescale of 0.3–1.0 Gyr (Barro et al. 2013). Deep near-infrared slit spectroscopy also suggests that their dynamical masses are comparable to their stellar masses, indicating a short quenching timescale (Barro et al. 2014b; Nelson et al. 2014). All these results point toward an evolutionary scenario in the fast mode, whereby extended SFGs evolve into compact SFGs through a violent starburst phase and then become compact QGs on a short quenching timescale.

In this Letter, we present 1.1 mm properties of SFGs at $z \sim 2$, along with the discovery of a galaxy with an extremely compact, dusty star-forming component. These are the first results from the SXDF-ALMA 1.5 arcmin^2 deep survey, which is unconfused (FWHM $= 0\farcs5$) and unbiased (i.e., blind) observations with ALMA. The ALMA observations target a part of the SXDF-UDS-CANDELS field, where *Hubble Space Telescope* (*HST*) high-resolution images are available (Grogin et al. 2011; Koekemoer et al. 2011). We only focus on 12 SFGs identified by a Hα narrowband imaging survey with the Subaru Telescope (Kodama et al. 2013; Tadaki et al. 2013). Survey design and source catalog of the ALMA observations are described in detail in Kohno et al. (in preparation). We assume the Chabrier initial mass function (Chabrier 2003) and adopt cosmological parameters of $H_0 = 70\,\mathrm{km\,s^{-1}\,Mpc^{-1}}$, $\Omega_\mathrm{M} = 0.3$, and $\Omega_\Lambda = 0.7$.

2. SAMPLE AND DATA

The SXDF-ALMA 1.5 arcmin^2 deep survey consists of 19 pointings (Figure 1). The Band 6 receivers were used in frequency ranges of 255–259 and 271–275 GHz ($\sim$1.1 mm). The data calibrations are performed using the Common Astronomy Software Application package (McMullin et al. 2007). We reconstruct a 1.1 mm continuum map with natural weighting. The synthesized beam size and the rms level before the primary beam correction are $0\farcs53 \times 0\farcs41$ and 55 μJy/beam, respectively.

The SXDF-ALMA 1.5 arcmin^2 deep field covers 11 Hα-selected SFGs at $z = 2.53$ and 1 at $z = 2.19$ (Figure 1). As they are carefully identified on the basis of the narrowband excess and the broadband colors for the line separation between Hα and [O III], the redshift ranges are strongly constrained by the width of narrowband filters, $\Delta z = \pm 0.02$. X-ray-detected active galactic nuclei or galaxies with a power-low spectral energy distribution (SED) at IRAC four bands are not included in our sample (Tadaki et al. 2013).

First, we model their SEDs to measure the rest-frame $U - V$ and $V - J$ color (*UVJ*) using the 3D-*HST* catalog with photometries at 18 bands (Skelton et al. 2014) and the EAZY code (Brammer et al. 2008). Next, we estimate the stellar mass and the amount of dust extinction for our sample by fitting the photometric SEDs with the stellar population synthesis model of Bruzual & Charlot (2003). The SED fitting is done using the FAST code (Kriek et al. 2009) with a solar metallicity, exponentially declining star formation histories (SFHs), and the dust attenuation law of Calzetti et al. (2000). Following the recipe presented by Wuyts et al. (2011a), we adopt a minimum *e*-folding time of 300 Myr. The uncertainties of the derived stellar mass are estimated from the 68% confidence interval. While the stellar mass tends to be the most robust parameter in SED modeling as long as single exponentially declining SFHs are assumed, the mass-to-light ratios could become smaller in two-component SFHs with recent bursts (Wuyts et al. 2007). The differences are smaller for redder galaxies because a new burst makes galaxies blue in the rest-frame optical. In Section 3.2, the stellar masses are used to determine dust temperatures. A higher stellar mass leads to a lower dust temperature and results in a higher gas mass, but does not significantly change it for red galaxies.

Star formation rates (SFRs) are derived from Hα luminosities (Kennicutt 1998) and SED-based extinctions, accounting for extra extinction toward H II regions (Wuyts et al. 2013). The [N II] contribution has been corrected on the basis of the measured equivalent width of Hα + [N II] emission lines (Tadaki et al. 2013). We have also applied UNIMAP (Piazzo et al. 2015) and extraction methods as described in Lutz et al. (2011) to the archival *Herschel*-PACS data. We detect one source NB2315-02 at $S_{160\,\mu\mathrm{m}} = 7.2 \pm 1.1$ mJy, corresponding to a total infrared luminosity of $\log (L_\mathrm{IR}/L_\odot) = 12.58$ using a conversion factor at $z = 2.53$ from PACS 160 μm to L_IR, based on the Wuyts et al. (2011a) template. The PACS 160 μm based SFR is $414 \pm 63\ M_\odot\,\mathrm{yr^{-1}}$, which is consistent with the Hα-based SFR of $495 \pm 95\ M_\odot\,\mathrm{yr^{-1}}$.

3. RESULTS

3.1. Detections in the 1.1 mm Continuum Map

As the 1.1 mm continuum emission of SFGs at $z \sim 2$ originates from thermal radiation of dust heated by massive stars, it serves as a good tracer of dusty star-forming regions within galaxies. For all 12 SFGs in our sample, we measure the flux densities within the $1\farcs5$ apertures and estimate the noise from 2000 random apertures ($1\sigma = 125$ μJy before the primary

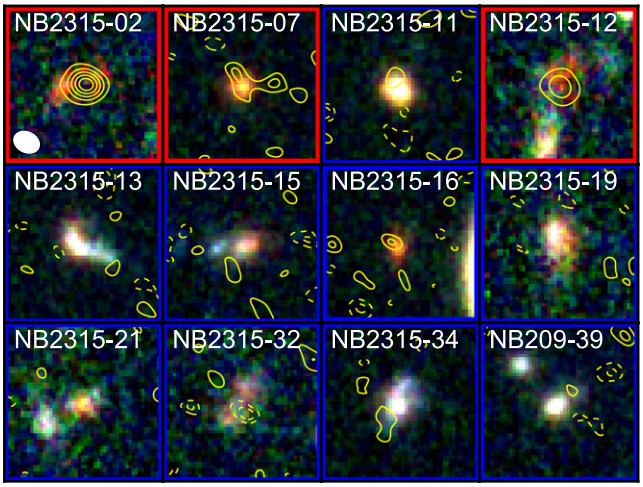

Figure 2. 1.1 mm continuum contours of our Hα-selected sample, superimposed on three-color images at the ACS/*F*814*W*, WFC3/*F*125*W*, and *F*160*W* bands ($3'' \times 3''$). Contours are plotted every 1σ, starting at 2σ, except for NB2315-02 and -12 (every 5σ). Dashed contours denote negative fluxes. The synthesized beam size is shown in the bottom left of the NB2315-02 panel.

beam correction). We adopt a 2σ detection criterion in the same manner as Scoville et al. (2014). The probabilities where a negative 2σ signal is detected by chance in the ALMA map are 2.2%. Three SFGs are associated with a 1.1 mm source with a $>2.6\sigma$ significance (Figure 2). NB2315-02 and NB2315-12 are robustly detected above 9σ, and NB2315-07 is marginally done at 2.6σ. The spurious detection rates of 2.6σ sources are 0.5%. Table 1 lists their measured flux densities along with stellar masses and SFRs. The other nine SFGs do not have a significant 1.1 mm continuum emission and their 2σ upper limit is $S_{1.1\,\mathrm{mm}} < 290$ μJy after the primary beam correction.

Our deep Hα narrowband selection covers wide ranges in colors and stellar mass of SFGs from blue, less massive to red, massive ones. The 1.1 mm detected SFGs are redder in the rest-frame optical and more massive than the non-detected sample (Figure 3). The *UVJ* diagram is useful for distinguishing between dusty star-forming, unobscured star-forming, and QGs (e.g., Wuyts et al. 2007). The three 1.1 mm sources are found to be dusty SFGs, while most of SFGs without 1.1 mm detection fall in the unobscured star-forming regime, where the bulk of galaxies satisfying the Lyman break criterion also lies. One galaxy, which lies in the regime where QGs dominate, is not detected above 2σ. NB2315-07 is also close to this regime compared to NB2315-02 and NB2315-12. Their lower position with respect to the main sequence supports that they are less SFGs. We stack the unconfused 1.1 mm maps in the positions of eight non-detected objects, excluding one less SFG, to investigate the existence of faint emission for typical main-sequence SFGs with $\log(M_*/M_\odot) = 10.0$–10.8. However, the deep stacked image does not show a significant emission and gives the 2σ upper limit of $S_{1.1\,\mathrm{mm}} < 100$ μJy.

3.2. Gas Mass Estimates

Measurements of 1.1 mm continuum flux densities, S_ν, allow us to derive gas masses of galaxies, although there are uncertainties associated with dust temperature variations (e.g., Scoville et al. 2014; Genzel et al. 2015). We estimate the gas mass of our sample using a modified blackbody radiation model as

$$M_{\mathrm{gas}} = M_{\mathrm{dust}}/\delta_{\mathrm{dgr}} = \frac{S_\nu d_{\mathrm{L}}^2}{\kappa_{\mathrm{ISM}} B_\nu\left(T_{\mathrm{dust}}\right)(1+z)}, \quad (1)$$

where δ_{dgr} is dust-to-gas ratio, κ_{ISM} is the dust opacity per unit mass of interstellar medium ($\propto\nu^\beta$), B_ν is the Plank function, T_{dust} is the dust temperature, and d_{L} is the luminosity distance. Here, $\kappa_{\mathrm{ISM},850\mu\mathrm{m}} = 4.84 \times 10^{-3}\,\mathrm{g^{-1}\,cm^2}$ and $\beta = 1.8$ are adopted (Scoville et al. 2014). We note that for local galaxies the scatter of dust-to-gas ratio is ± 0.28 dex at fixed metallicities (Rémy-Ruyer et al. 2014). Although a conversion from monochromatic submillimeter luminosity to gas mass (i.e., κ_{ISM}) is not straightforward, observations of dust emission still have a big cost advantage over CO observations. Genzel et al. (2015) present scaling relations of dust temperature, gas fraction, and gas depletion timescale by compiling CO and dust continuum data for each of the ~500 galaxies over $0 < z < 3$ and find dust temperatures to only change slowly with specific SFR (sSFR) in the narrow range around the main sequence (see also Magnelli et al. 2014). This scaling relation of dust temperatures is used for better estimates of the rest-frame 850 μm fluxes from the observed 1.1 mm fluxes. The derived dust temperatures are 33^{+3}_{-2}, 28 ± 2, and 30 ± 2 K for NB2315-02, -07, and -12. The estimated gas masses and gas fractions, $f_{\mathrm{gas}} = M_{\mathrm{gas}}/(M_{\mathrm{gas}} + M_*)$, are summarized in Table 1.

The 2σ upper limit of our 1.1 mm survey corresponds to a gas mass of $\log(M_{\mathrm{gas}}/M_\odot) = 10.2$ in $T_{\mathrm{dust}} = 30$ K at $z = 2.53$. Surprisingly, we do not detect the 1.1 mm emission from relatively less massive SFGs around the main sequence, although their gas mass is expected to be $\log(M_{\mathrm{gas}}/M_\odot) = 10.1$–10.8 based on the CO-based scaling relations of gas fraction with redshift, SFR, and stellar mass (Genzel et al. 2015). The non-detection could be partly caused by the usage of the fixed $\kappa_{\mathrm{ISM}}(=\kappa_{\mathrm{dust}}\delta_{\mathrm{dgr}})$, where the term of δ_{dgr} is canceled out on the right side of Equation (1). SFGs with lower metallicity should be fainter at 1.1 mm due to a lower dust-to-gas ratio than metal-rich ones, $\log\delta_{\mathrm{dgr}} = -2 + 0.85 \times (12+\log(\mathrm{O/H}) - 8.67)$ (Leroy et al. 2011), even if they have the same gas mass. The mass–metallicity relation at $z \sim 2$ predicts $\log\delta_{\mathrm{dgr}} = -2.3$ for SFGs with $\log(M_*/M_\odot) = 10$ (Wuyts et al. 2014). Moreover, although the used dust opacity has been calibrated mainly by using outliers above the main sequence such as local ultraluminous infrared galaxies and bright SMGs at $z \sim 2$ (Scoville et al. 2014), it is not necessarily appropriate for less massive normal SFGs at $z \sim 2$. Diffuse dust distributions within galaxies could lead to a low dust opacity (Dunne et al. 2003), resulting in faint 1.1 mm emission at fixed gas mass. Also, dust SEDs of SFGs are better described by a multi-temperature model including cool dust in diffuse ISM (dominating a dust mass) and warm dust in birth clouds (dominating a total infrared luminosity). Local normal SFGs have a cold component with $T_{\mathrm{dust}} \sim 20$ K in a two-temperature model, while a single-temperature model shows higher dust temperatures (Dunne et al. 2011).

Assuming $\log\delta_{\mathrm{dgr}} = -2.3$, $\kappa_{\mathrm{dust},850\mu\mathrm{m}} = 0.4\,\mathrm{g^{-1}\,cm^2}$ (Dunne et al. 2003), and $T_{\mathrm{dust}} = 20$ K, the 2σ gas mass limit of our observations would become $\log(M_{\mathrm{gas}}/M_\odot) = 11.0$. As the non-detections for less massive galaxies can be explained by a combination of these factors, it is difficult to determine

Table 1
Properties of 1.1 mm Detected SFGs

ID	R.A. (J2000)	Decl. (J2000)	z_{NB}	M_* ($10^{10}\,M_\odot$)	$SFR_{H\alpha}$ ($M_\odot\,yr^{-1}$)	$S_{1.1mm,aper}$ (mJy)	M_{gas} ($10^{10}\,M_\odot$)	f_{gas} (%)
NB2315-02	02 17 40.53	−05 13 10.7	2.53 ± 0.02	$13.1^{+4.8}_{-8.0}$	495 ± 95	2.06 ± 0.13	$10.3^{+1.7}_{-1.5}$	44^{+20}_{-8}
NB2315-07	02 17 42.67	−05 13 58.4	2.53 ± 0.02	$8.9^{+0.9}_{-0.8}$	49 ± 10	0.38 ± 0.15	$2.7^{+1.2}_{-1.0}$	23^{+8}_{-8}
NB2315-12	02 17 41.11	−05 13 15.2	2.53 ± 0.02	$17.5^{+1.4}_{-2.2}$	174 ± 20	1.34 ± 0.15	$8.1^{+1.8}_{-1.3}$	32^{+5}_{-4}

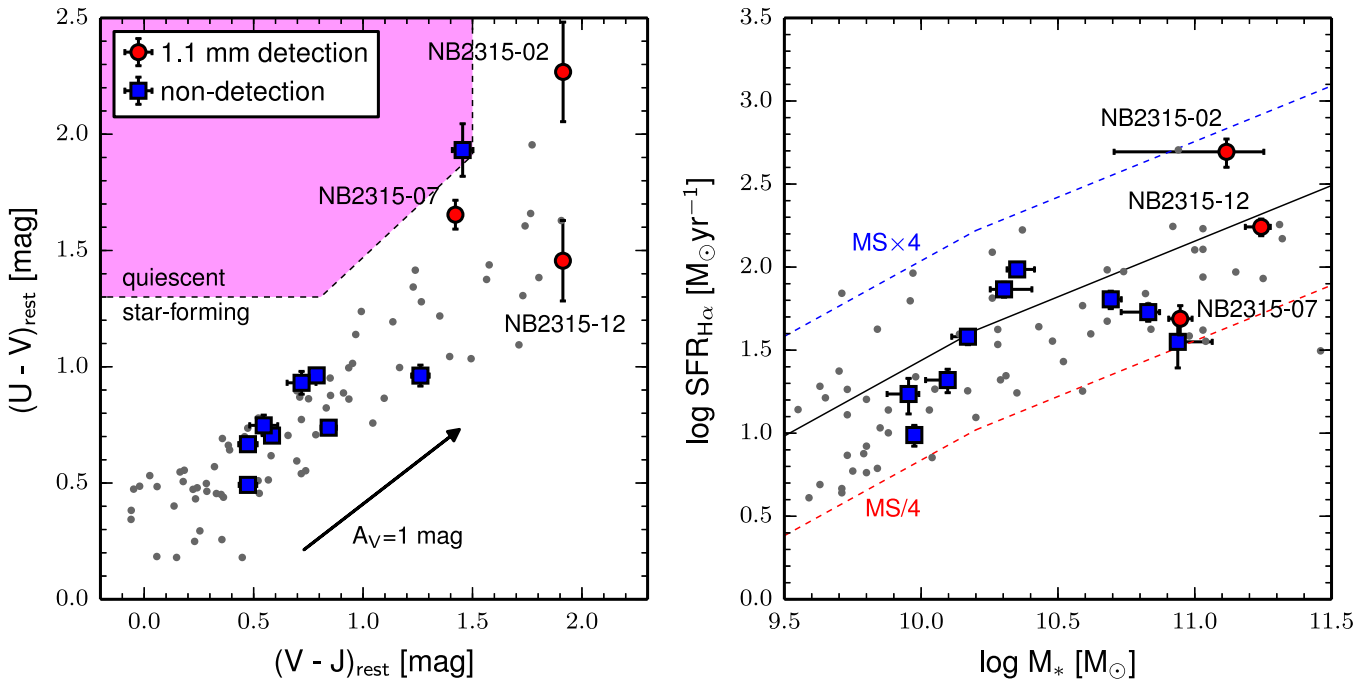

Figure 3. Left: rest-frame $U-V$ vs. $V-J$ color for our sample. Red circles and blue squares indicate 1.1 mm detected and non-detection sources, respectively. Gray circles show the parent sample of Hα-selected SFGs. The red shaded area indicates a region where quiescent galaxies dominate (Whitaker et al. 2011). Right: Hα-based star formation rates plotted against stellar masses. The black solid line indicates the main sequence of SFGs at $z = 2.0$–2.5 (Whitaker et al. 2014).

whether the gas mass is actually as small as log ($M_{gas}/M_\odot$) = 10.2 with the 1.1 mm data alone.

3.3. Size Measurements of Dust Emission

We measure the size of the dust emission for two 1.1 mm bright galaxies (NB2315-02 and NB2315-12) by fitting the visibility data in the *uv* plane. Their signal-to-noise ratios in the 1.1 mm map are >10 in the flux density per synthesized beam to reliably constrain the size as the visibility coverage is similar to those of Ikarashi et al. (2014) and Simpson et al. (2015). Then, we assume two models, a circular Gaussian component, and a point source. The `uvamp` task in MIRIAD (Sault et al. 1995) is used for calculating the visibility amplitudes averaged in annuli according to the *uv* distance after shifting the phase center to the center position measured in the image plane and subtracting a clean component of another source in the primary beam with the `uvmodel` task. The phase calibrator, J0215-0222, shows constant amplitudes as a function of *uv* distance, suggesting a point source in the used antenna configuration (Figure 4). On the other hand, two SFGs of our sample seem to be resolved at >300 kλ. The Gaussian fitting shows reduced chi-square values of 0.61 for NB2315-02 and 1.62 for NB2315-12, while the horizontal fitting (point source) shows 5.76 and 2.60, respectively. Therefore, we adopt the Gaussian model that is the same approach as previous studies (Ikarashi et al. 2014; Simpson et al. 2015). The best-fit results are FWHM = $0\farcs16^{+0.03}_{-0.02}$ ($R_e = 0.66\pm^{+0.11}_{-0.08}$ kpc) for NB2315-02 and FWHM = $0\farcs20^{+0.06}_{-0.04}$ ($R_e = 0.81^{+0.25}_{-0.15}$ kpc) for NB2315-12. NB2315-02 surely has a compact, dusty star-forming component with $R_e < 1$ kpc at 3σ significance. For a Gaussian source with $R_e = 0.66\pm^{+0.11}_{-0.08}$ kpc, 80^{+7}_{-11}% ($SFR_{H\alpha} = 396^{+84}_{-93}\ M_\odot\,yr^{-1}$) of star formation traced by Hα is occurring within 1 kpc region. Then, the SFR surface density could be $126^{+27}_{-30}\ M_\odot\,yr^{-1}\,kpc^{-2}$. It is also $105^{+19}_{-22}\ M_\odot\,yr^{-1}\,kpc^{-2}$ in the case of usage of the PACS 160 μm based SFR. The gas surface density is similarly estimated from the total gas mass to be (2.6 ± 0.5) × $10^{10}\ M_\odot\,kpc^{-2}$, which probably causes an extremely red color due to strong extinction (Figure 3).

4. DISCUSSION

We find NB2315-02 to have a high SFR surface density, $126^{+27}_{-30}\ M_\odot\,yr^{-1}\,kpc^{-2}$, corresponding to $SFR = 396^{+84}_{-93}\ M_\odot\,yr^{-1}$ within a region of 1 kpc radius. The central stellar surface density will become comparable with compact SFGs/QGs, $\log(M_*/R_e^{1.5}) > 10.3$ [$M_\odot\,kpc^{-1.5}$] (Barro et al. 2013), provided that the current star formation is maintained for another 50^{+12}_{-11} Myr in the galaxy center. This is plausible since it would need only 19 ± 3% of the total gas mass ($M_{gas} = 10.3^{+1.7}_{-1.5} \times 10^{10}\ M_\odot$) being converted into stars. Then, the gas

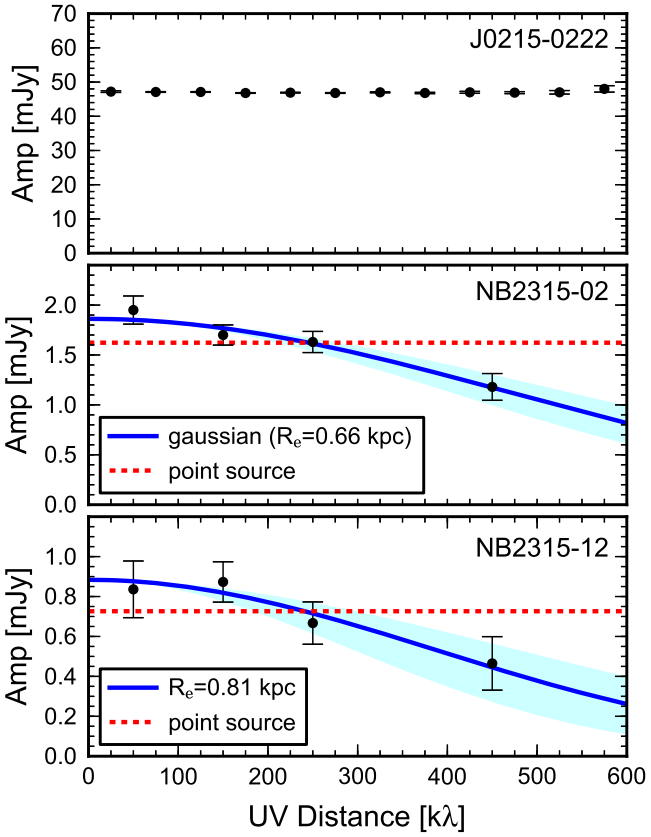

Figure 4. Visibility amplitudes averaged over *uv* distances for the phase calibrator, J0215-0222 (top), NB2315-02 (middle), and NB2315-12 (bottom). A blue solid line and a shaded region indicate the best-fitting circular Gaussian component and the 1σ error, respectively. A red dashed line presents the best-fitting point-source model as a reference.

depletion timescale, $\tau_{\rm depl} \equiv M_{\rm gas}/{\rm SFR}_{\rm H\alpha}$, is 207^{+78}_{-44} Myr. Barro et al. (2014b) have also estimated dynamical masses of 13 compact SFGs from line widths of nebular emission (Hα or [O III]) by near-infrared slit spectroscopy and derived similar gas depletion timescales ($\tau_{\rm depl} = 230^{+110}_{-190}$ Myr). The agreement of the gas depletion timescales would support that the compact, dusty SFG can be an immediate progenitor of the high stellar surface density SFGs.

In the WFC3/*F*160*W*-band image, NB2315-02 has a subcomponent with log $(M_*/M_\odot) = 10.67$, which is seen 5 kpc east of the main component with the Hα peak (Figure 2). The compact starburst region appears to be located in between the two components. Given the high gas surface density of $(2.6 \pm 0.5) \times 10^{10}\ M_\odot\,{\rm kpc}^{-2}$ in the compact, dusty SFG, the rest optical morphology may be severely affected by strong attenuation. One likely interpretation is that the two components would constitute a single large SFG with a central dusty star formation. The gas fraction becomes 37^{+25}_{-3}% in this system, including the companion. A physical process to reduce angular momentum is required in order to explain a concentrated gas distribution in a center of extended SFGs. In gas-rich disks at $z \sim 2$, gravitational torques and dynamical friction due to clumps can drive angular momentum out and cause mass inflow toward galaxy centers (Dekel & Burkert 2014; Zolotov et al. 2015). Then, if the inflow timescale is shorter than the star formation timescale, a gas-rich, central starburst may form. The measured high gas fraction of the compact, dusty SFG could support the possibility of such a dissipational process. Another possible explanation is we are witnessing a late-stage merger with 1:3 stellar mass ratio immediately before the final coalescence. Numerical simulations demonstrate that gas-rich mergers produce an instantaneous starburst at the final coalescence although it depends on merger parameters such as orbits of the two galaxies (Hopkins et al. 2013).

As compact SFGs are commonly defined not by high gas/dust surface densities but by stellar ones (Barro et al. 2013, 2014a), they are likely to have already completed most of the morphological transformation from extended disks to compact spheroids, while compact, dusty SFGs have not yet finished. NB2315-07 of our sample shows a compact morphology with a circularized, effective radius of $R_{\rm e} = 1.43 \pm 0.03$ kpc at the *F*160*W* band (van der Wel et al. 2014) and satisfies the conditions for compact SFGs, $\log(M_*/R_{\rm e}^{1.5}) = 10.71^{+0.05}_{-0.04} > 10.3$ $[M_\odot\,{\rm kpc}^{-1.5}]$ and $\log({\rm SFR}_{\rm H\alpha}/M_*) = -0.26 \pm 0.10 > -1.0\,[{\rm Gyr}^{-1}]$ (Barro et al. 2014a). The 1.1 mm based gas fraction is 23^{+8}_{-8}%, which is smaller than that of the compact dusty SFG at 2σ significance. Given the observed lower gas fraction and less star-forming properties shown in Figure 3, this compact less SFG is likely already in a late stage of their evolutionary path to a compact QG.

In the fast quenching mode for galaxy evolution, we are looking various compact objects in different evolutionary phases from dusty to quiescent to star-forming galaxies. Barro et al. (2014a) also present a variety of compact SFGs from highly obscured (they are similar to compact, dusty SFGs but already have a compact stellar core) to less star-forming ones (to which NB2315-07 belongs). The spatial extent of gas remaining within galaxies can provide key information about the subsequent evolution of compact SFGs. If gas is still concentrated in a galaxy center, compact SFGs are expected to exhaust all gas by a nuclear starburst or a feeding to a supermassive black hole and then quench star formation. Deep and high-resolution submillimeter imaging with ALMA has great potential to address this issue.

We thank the anonymous referee, who gave us a number of comments that improved the Letter. This Letter makes use of the following ALMA data: ADS/JAO.ALMA#2012.1.00756. S. ALMA is a partnership of ESO (representing its member states), NSF (USA) and NINS (Japan), together with NRC (Canada), NSC and ASIAA (Taiwan), and KASI (Republic of Korea), in cooperation with the Republic of Chile. The Joint ALMA Observatory is operated by ESO, AUI/NRAO and NAOJ. This work is based on observations taken by the 3D-*HST* Treasury Program (GO 12177 and 12328) with the NASA/ESA *HST*, which is operated by the Association of Universities for Research in Astronomy, Inc., under NASA contract NAS5-26555. Data analysis was in part carried out on the common use data analysis computer system at the Astronomy Data Center, ADC, of the National Astronomical Observatory of Japan. This work was supported by JSPS KAKENHI Grant Numbers 21340045, 24244015, and 25247019. R.J.I. acknowledges support in the form of the ERC Advanced Grant, COSMICISM.

REFERENCES

Barro, G., Faber, S. M., Pérez-González, P. G., et al. 2013, ApJ, 765, 104
Barro, G., Faber, S. M., Pérez-González, P. G., et al. 2014a, ApJ, 791, 52

Barro, G., Trump, J. R., Koo, D. C., et al. 2014b, ApJ, 795, 145
Belli, S., Newman, A. B., & Ellis, R. S. 2015, ApJ, 799, 206
Bournaud, F., Chapon, D., Teyssier, R., et al. 2011, ApJ, 730, 4
Brammer, G. B., van Dokkum, P. G., & Coppi, P. 2008, ApJ, 686, 1503
Bruzual, G., & Charlot, S. 2003, MNRAS, 344, 1000
Calzetti, D., Armus, L., Bohlin, R. C., et al. 2000, ApJ, 533, 682
Chabrier, G. 2003, PASP, 115, 763
Dekel, A., & Burkert, A. 2014, MNRAS, 438, 1870
Dunne, L., Eales, S., Ivison, R., Morgan, H., & Edmunds, M. 2003, Natur, 424, 285
Dunne, L., Gomez, H. L., da Cunha, E., et al. 2011, MNRAS, 417, 1510
Genzel, R., Tacconi, L. J., Lutz, D., et al. 2015, ApJ, 800, 20
Grogin, N. A., Kocevski, D. D., Faber, S. M., et al. 2011, ApJS, 197, 35
Hopkins, P. F., Cox, T. J., Hernquist, L., et al. 2013, MNRAS, 430, 1901
Ikarashi, S., Ivison, R. J., Caputi, K. I., et al. 2014, ApJ, in press (arXiv:1411.5038)
Kennicutt, R. C., Jr. 1998, ARA&A, 36, 189
Kodama, T., Hayashi, M., Koyama, Y., et al. 2013, in IAU Symp. 295, The Intriguing Life of Massive Galaxies, ed. D. Thomas, A. Pasquali, & I. Ferreras (Cambridge: Cambridge Univ. Press), 74
Koekemoer, A. M., Faber, S. M., Ferguson, H. C., et al. 2011, ApJS, 197, 36
Kriek, M., van Dokkum, P. G., Labbé, I., et al. 2009, ApJ, 700, 221
Leroy, A. K., Bolatto, A., Gordon, K., et al. 2011, ApJ, 737, 12
Lutz, D., Poglitsch, A., Altieri, B., et al. 2011, A&A, 532, A90
Magnelli, B., Lutz, D., Saintonge, A., et al. 2014, A&A, 561, A86
McMullin, J. P., Waters, B., Schiebel, D., Young, W., & Golap, K. 2007, in ASP Conf. Ser. 376, Astronomical Data Analysis Software and Systems XVI, ed. R. A. Shaw, F. Hill, & D. J. Bell (San Francisco, CA: ASP), 127
Naab, T., Johansson, P. H., & Ostriker, J. P. 2009, ApJL, 699, L178
Nelson, E., van Dokkum, P., Franx, M., et al. 2014, Natur, 513, 394
Newman, A. B., Ellis, R. S., Bundy, K., & Treu, T. 2012, ApJ, 746, 162
Piazzo, L., Calzoletti, L., Faustini, F., et al. 2015, MNRAS, 447, 1471
Rémy-Ruyer, A., Madden, S. C., Galliano, F., et al. 2014, A&A, 563, A31
Sault, R. J., Teuben, P. J., & Wright, M. C. H. 1995, in ASP Conf. Ser. 77, Astronomical Data Analysis Software and Systems IV, ed. R. A. Shaw, H. E. Payne, & J. J. E. Hayes (San Francisco, CA: ASP), 433
Scoville, N., Aussel, H., Sheth, K., et al. 2014, ApJ, 783, 84
Simpson, J. M., Smail, I., Swinbank, A. M., et al. 2015, ApJ, 799, 81
Skelton, R. E., Whitaker, K. E., Momcheva, I. G., et al. 2014, ApJS, 214, 24
Tadaki, K.-i., Kodama, T., Tanaka, I., et al. 2013, ApJ, 778, 114
Tadaki, K.-i., Kodama, T., Tanaka, I., et al. 2014, ApJ, 780, 77
Trujillo, I., Conselice, C. J., Bundy, K., et al. 2007, MNRAS, 382, 109
van der Wel, A., Franx, M., van Dokkum, P. G., et al. 2014, ApJ, 788, 28
van Dokkum, P. G., Franx, M., Kriek, M., et al. 2008, ApJL, 677, L5
van Dokkum, P. G., Whitaker, K. E., Brammer, G., et al. 2010, ApJ, 709, 1018
Wellons, S., Torrey, P., Ma, C.-P., et al. 2015, MNRAS, 449, 361
Whitaker, K. E., Franx, M., Leja, J., et al. 2014, ApJ, 795, 104
Whitaker, K. E., Labbé, I., van Dokkum, P. G., et al. 2011, ApJ, 735, 86
Williams, R. J., Quadri, R. F., Franx, M., et al. 2010, ApJ, 713, 738
Wuyts, E., Kurk, J., Förster Schreiber, N. M., et al. 2014, ApJL, 789, L40
Wuyts, S., Cox, T. J., Hayward, C. C., et al. 2010, ApJ, 722, 1666
Wuyts, S., Förster Schreiber, N. M., Lutz, D., et al. 2011a, ApJ, 738, 106
Wuyts, S., Förster Schreiber, N. M., Nelson, E. J., et al. 2013, ApJ, 779, 135
Wuyts, S., Förster Schreiber, N. M., van der Wel, A., et al. 2011b, ApJ, 742, 96
Wuyts, S., Labbé, I., Franx, M., et al. 2007, ApJ, 655, 51
Zolotov, A., Dekel, A., Mandelker, N., et al. 2015, MNRAS, 450, 2327